ICAS 2020 SHANG HAI
International Council of the Aeronautical Sciences
32nd Congress of the International Council of the Aeronautical Sciences
September 6-10, 2021
Pudong Shangri-La, Shanghai, China

Multifidelity Aerodynamic/Stealth Design Optimization Method for Flying Wing Aircraft

Ziqiao Liu, Wenping Song, Zhonghua Han*, Yuan Wang

Institute of Aerodynamic and Multidisciplinary Design Optimization
National Key Laboratory of Science and Technology on Aerodynamic Design and Research
School of Aeronautics, Northwestern Polytechnical University

Abstract

The design optimization considering both aerodynamic and stealth performances has been an important and challenging area for next-generation aircraft. One of the main difficulties is associated with the prohibitive computational cost of optimization with a large number of design variables. A two-rounds multi-fidelity aerodynamic/stealth design optimization method based on hierarchical Kriging (HK) model is developed in this paper by using the validated RANS solver and computational electromagnetics (CEM) methods based on the multilevel fast multipole algorithm (MLFMA) and physical optics (PO) algorithm. RANS method with fine grids and MLFMA method are used as high-fidelity CFD/CEM simulation. RANS method with coarse grids and PO method are served as low-fidelity CFD/CEM simulation. A low-fidelity optimization based on Kriging model is carried out to get lots of low-fidelity sample data which are used by HK model. The optimum shape is simulated by high-fidelity CFD/CEM methods to get the data used as high-fidelity sample points of the HK model. At the same time, some new initial high-fidelity sample points are generated by Latin hypercube sampling (LHS) method. The two kinds of high-fidelity sample points and lots of low-fidelity sample points are used to build initial HK model. Then an aerodynamic/stealth coupled design optimization of a flying wing aircraft with 108 design variables is carried out to validate effectiveness of the method. The objective is to reduce total drag of cruise condition and frontal RCS. Results indicate that with the method developed in this paper, the efficiency of aerodynamic/stealth optimization is improved significantly. The number of high-fidelity CFD/CEM simulations is reduced by seven times. Only 39 CFD/CEM simulations are used to get the optimum shape. The drag coefficient of optimized flying wing at a cruise condition is reduced by 3.5% and the average RCS in the frontal observation angle range is reduced by 44.3%, which validates the effectiveness of the developed method.

Keywords: Aerodynamic shape optimization, Aerodynamic/stealth optimization, Surrogate-based optimization, Flying wing , Computational fluid dynamics

1. Introduction

Low radar cross section (RCS) has been viewed as one of the most important feature of next-generation aircraft. Tailless configuration such as flying wing is regarded as an ideal layout to get lower radar signature and shorten detection range in all directions-especially in the lateral direction. Compared with the characteristic length of flying wing, the wavelength of modern radars is much smaller. The frequency bands of radar, that are commonly used to detect aircraft, are L,S,C and X bands. Their working frequencies vary from 1GHz to 12GHz, which belong to a high-frequency region. For scatter problems in high-frequency region, since aircraft shape is the primary factor to reduce radar cross section(RCS), meanwhile, shape details also have a great influence on aerodynamic performance, a coupled design optimization method to balance the two kinds of performance is urgently required.

Many meaningful studies on design optimization methods have been conducted during the last decades. They can be divided into gradient-based and gradient-free methods. The advantage of gradient-based methods is that they require significantly smaller number of function evaluations, but

the difficulty lies on time consuming gradient calculations. To solve this problem, adjoint method [1] whose computational time of calculating gradient is nearly independent of design variables, has been applied to get the gradients of objective functions for different disciplines, such as aerodynamics [2], structure [3], and etc. Some researchers have successfully applied adjoint method to get the gradients of RCS in recent years. Wang et al. [4] developed a time-dependent discrete adjoint method based on the high-order discontinuous Galerkin (DG) method for electromagnetic scattering problems. Huang et al. [3] developed a multidisciplinary coupled adjoint system between aerodynamics and electromagnetics, including electromagnetic adjoint equations and aerodynamic/electromagnetic coupled adjoint equations. Based on these researches, Zhou et al. [5] developed a discrete adjoint method based on multilevel fast multipole algorithm (MLFMA) to calculate the gradients of RCS, which was applied to aerodynamic/stealth shape design optimization of a blend-wing-body (BWB). The research indicated that conflictions between leading edge with small radius and drag reduction are not very prominent at cruise condition, and the leading edge with small radius is beneficial to reduce RCS. Li et al. [6] developed an aerodynamic/ stealth optimization system for a certain flying wing aircraft, with discrete adjoint method based on Reynolds-Averaged Navier-Stokes (RANS) equations and automatic differentiation (AD) technology based on physical optics (PO) method. The influence of weight factors on aerodynamic/stealth optimization was also discussed in the paper.

Though gradient-based methods require significantly smaller number of function evaluations, but they can't find the global optimum theoretically. The studies on gradient-free methods are still necessary for aerodynamic/stealth optimization. Genetic algorithm (GA) is one of most popular gradient-free methods and has been widely used in aerodynamic/stealth shape design optimization of aircraft. In 1999, Mäkinen et al. [7] used GA, the finite volume discretization of Euler equations, and two-dimensional Helmholtz equation to study aerodynamic/stealth design optimization of airfoil. In 2008, D.S.Lee et al. [8] applied robust evolutionary algorithms to aerodynamic/stealth shape design optimization of UAV. In 2017, Xia et al. [9] applied rank altered differential particle swarm optimization (RADPSO) to design stealth airfoils for inner wing and outer wing of a flying wing configuration, in their paper, the flow solver was based on RANS equations and the RCS solver is based on PO method. Although GA has great ability to find the global optimum, but its computational cost of global optimization is prohibitive when high-fidelity aerodynamic/ electromagnetic simulation such as RANS and MLFMA method is adopted, especially for the optimization with more than 30 design variables. In this context, surrogate-based optimization (SBO) [10][11], as a generalization of efficient global optimization method, has been developed. It was widely used in the aerodynamic design optimization and multidisciplinary design optimization [14][17] of aircrafts such as hypersonic vehicle[12], transonic transport aircraft[13][15][16][18]~[21], helicopter[22][23], and supersonic civil aircraft[24]. In aspect of aerodynamic/stealth design optimization of aircraft， Zhang et al. [25] developed an adaptive design space expansion method based on Kriging model，which was applied on aerodynamic/stealth optimization of NACA65,3-018 airfoil. The design space is dynamic and able to be expanded in the range of the most sensitive design variables. Chen et al. [26] used radial basis function (RBF) neural network to build surrogate model and used multi-objective genetic algorithm (MOGA) to get pareto solutions of stealth airfoil. The research indicated that design of stealth airfoil for flying wing aircraft is important and the airfoils with "eagle beak" leading edge can reduce RCS in frontal. Jiang et al. [27] built RBF surrogate model to optimize the aerodynamic and stealth performances of rotor. In their work, the CFD method is RANS equations with Spalart-Allmaras (S-A) turbulence model, the CEM method is PO with method of equivalent currents (MEC) and method of quasi stationary (MQS). Gao et al. [29] adopted double-stage metamodel (DSM) that integrates advantages of both interpolation and regression metamodel to optimize a flying wing UAV, where RANS equations method with S-A turbulence model was used in CFD numerical simulation and the spare-matrix method (SMM) [30] was adopted to calculate RCS. Xu et al. [35] proposed a stealth inverse design method for twin-engine layout flying wing UAV and a kind of fuselage with leading edge similar to eagle mouth, their results confirmed that the leading edge similar to eagle mouth is helpful to improve both aerodynamic and stealth performance.

All of the studies about gradient-free methods mentioned above only use single fidelity CFD/CEM simulation methods. Although SBO method is more efficient compared with GA [10], the

major difficulty of SBO lies on that its efficiency is low for high-dimensional global optimization, especially for the problems with more than 100 design variables. Therefore, some meaningful researches have been done to solve this problem. Some researches combined gradients and surrogate model to build gradient-enhanced surrogate model such as gradient-enhanced Kriging (GEK) [18][28]. By adopting adjoint method to get gradients of sample data [21], the number of time-consuming simulation such as CFD can be reduced significantly. The other idea is to use low-fidelity, cheaper function to assist the prediction of a high-fidelity, expensive function, by which variable-fidelity model (VFM) is built. Variable-fidelity Kriging is one of the most popular techniques for VFM, such as Cokriging [31][33] and Hierarchical Kriging (HK) [32]. In 2012, Han [32] proposed a simple and robust VFM called Hierarchical Kriging. It uses the estimated value of the low-fidelity model as a global trend function in the process of building the high-fidelity model. Compared with the traditional Cokriging model, HK model can provide more reasonable Mean-Squared-Error (MSE) estimation and can be more accurate with the same sample points. However, HK model only has two levels of fidelity and the efficiency improvement is limited. In 2020, Han et al. [34] proposed a Multi-level Hierarchical Kriging (MHK) model based on HK model. The fidelity levels of MHK were extended to three or more fidelities by comparison with HK model. The results of aerodynamic optimization with MHK model confirmed that the optimization efficiency with three-level-fidelity CFD simulations can be significantly improved compared with traditional single-fidelity or two-level-fidelity method. In aspect of engineering, the variable-fidelity method with HK model has been successfully adopted in aerodynamic/aeroacoustic optimization of helicopter rotor [23], with which the computational time of rotor design optimization was reduced by 35%.

As a summary of literature review, it is observed that global aerodynamics/stealth coupled design optimization based on gradient-free method such as SBO suffers from low efficiency when the number of design variables is increased up to about 30 and beyond. It requires large number of high-fidelity CFD/CEM simulations such as RANS and MLFMA. However, sufficient number of design variables are necessary for the complex aerodynamics/stealth coupled design of whole aircraft. The purpose of present work is to develop an efficient global multi-fidelity aerodynamics /stealth coupled design optimization method with HK model, which is suitable for three-dimensional aerodynamic/stealth optimization with more than 100 design variables and can significantly reduce number of high-fidelity CFD/CEM simulation.

This paper is organized as follows. In Sec. 2, the formulation of HK model and a multi-fidelity aerodynamic/stealth design optimization strategy based on HK model are derived. The accuracy of CFD/CEM solver are validated with benchmark case. In Sec. 3, the method is adopted for aerodynamics/stealth coupled design optimization of a flying wing aircraft with 108 design variables. At last, in Sec. 4, general conclusions will be drawn.

2. Multifidelity Aerodynamic/Stealth Shape Design Optimization Method

2.1 Hierarchical Kriging model

The HK method is a modeling strategy based on Kriging model for different fidelity analysis. High-fidelity analysis usually uses more complex physical models and finer computation grids. The calculated results are more accurate, but the time costs are higher. The low-fidelity analysis uses simplified conditions, empirical formulas or coarse grids in the process of simulation. The accuracy of analysis is low than that of high-fidelity analysis, but its calculation time is much shorter. In this condition, building HK model is able to make the best advantages of different fidelity analysis. The assumption of HK model is that low-fidelity analysis can provide similar trends to the results of high-fidelity analysis. The main idea is to use lots of low-fidelity data building global trend model, and use few high-fidelity data to modify the global trend model. With this modeling strategy, the number of high-fidelity sample points is reduced, and the convergence solution is obtained faster than Kriging model.

Before building a surrogate model for high-fidelity function, we build a Kriging model for low-fidelity function firstly to assist prediction. Assume that a random process corresponding to the low-fidelity function $\hat{y}_{lf}(\boldsymbol{x})$ is as follows:

$$y_{lf}\left(\boldsymbol{x}\right)=\beta_{0,lf}+\boldsymbol{r}_{lf}^{T}\left(\boldsymbol{x}\right)\boldsymbol{R}_{lf}^{-1}\left(\boldsymbol{y}_{S,lf}-\beta_{0,lf}\boldsymbol{F}\right) \tag{1}$$

where

$$\begin{cases} \boldsymbol{R}_{lf} = \left(R\left(\boldsymbol{x}^{(i)}, \boldsymbol{x}^{(j)} \right) \right)_{i,j} \in \mathbb{R}^{n?n} \\ \boldsymbol{r}_{lf} = \left(R\left(\boldsymbol{x}^{(i)}, \boldsymbol{x} \right) \right)_{i} \in \mathbb{R}^{n} \\ \boldsymbol{F}_1 = \left[1,1,1,\ldots 1 \right]^T \\ \beta_{0,lf} = \left(\boldsymbol{F}_1^{\,T} \boldsymbol{R}_{lf}^{-1} \boldsymbol{F}_1 \right)^{-1} \boldsymbol{F}_1^{\,T} \boldsymbol{R}_{lf}^{-1} \boldsymbol{y}_{S,lf} \end{cases} \tag{2}$$

$\boldsymbol{R}_{lf}$ is the correlation matrix representing the correlation between the observe points; $\boldsymbol{F}_1$ is a column vector filled with digital one; $\boldsymbol{r}_{lf}$ is the correlation vector representing the correlation between the untried point and the observed points. $\boldsymbol{y}_{S,lf}$ is response values. For details of building such a Kriging, please refer to Ref. [11].

The next step is to build Hierarchical Kriging of high-fidelity function. Different from conventional Kriging mod-el, the low-fidelity Kriging model is employed as a trend function. We assume that the random process corresponding to the high-fidelity function is of the form:

$$Y(\boldsymbol{x}) = \beta_0 \hat{y}_{lf}(\boldsymbol{x}) + Z(\boldsymbol{x}) \tag{3}$$

The approximated low-fidelity function $\hat{y}_{lf}(\boldsymbol{x})$ scaled by unknown constant factor β_0 serves as the global trend function. The HK predictor of $y(\boldsymbol{x})$ at an untried $\boldsymbol{x}$ is formally defined as :

$$\hat{y}(\boldsymbol{x}) = \boldsymbol{w}^T \boldsymbol{y}_S \tag{4}$$

where

$$\begin{aligned} \boldsymbol{y}_S &= \left[y^{(1)}, y^{(2)}, \cdots, y^{(n)} \right]^T \\ \boldsymbol{w} &= \left[w^{(1)}, w^{(2)}, \ldots, w^{(n)} \right]^T \end{aligned} \tag{5}$$

$\boldsymbol{y}_S$ is the observed functional response at high-fidelity level and $\boldsymbol{w}$ is a vector of weight coefficients associated with the sampled high-fidelity data. Then we replace $\boldsymbol{y}_S$ with its corresponding random quantities $\boldsymbol{Y}_S = \left[Y^{(1)}, Y^{(2)}, \cdots, Y^{(n)} \right]^T$, $\boldsymbol{Y}_S$ satisfies the following unbiased estimation condition:

$$E\left[\sum_{i=1}^{n} w^{(i)} Y\left(\boldsymbol{x}^{(i)} \right) \right] = E\left[Y(\boldsymbol{x}) \right] \tag{6}$$

The mean square error (MSE) of HK model can be expressed as:

$$\begin{aligned} MSE\left[\hat{y}(\boldsymbol{x}) \right] &= E\left[\left(\boldsymbol{w}^T \boldsymbol{Y}_S - Y(\boldsymbol{x}) \right)^2 \right] \\ &= \sigma^2 \left(1 + \boldsymbol{w}^T \boldsymbol{R} \boldsymbol{w} - 2 \boldsymbol{w}^T \boldsymbol{r} \right) \end{aligned} \tag{7}$$

Under the unbiased estimation condition, the MSE is minimized to obtain the optimal weight coefficient. We use the Lagrangian multiplier method to solve this minimization problem, which solves the following equations:

$$min \;\; f(\boldsymbol{w}, \mu) = \left[\sigma^2 \left(1 + \boldsymbol{w}^T \boldsymbol{R} \boldsymbol{w} - 2 \boldsymbol{w}^T \boldsymbol{r} \right) \right] - \mu \left[\sum_{i=1}^{n} w^{(i)} - 1 \right] \tag{8}$$

The Lagrange multiplier μ and the weight coefficients $\boldsymbol{w}$ can be found by solving the following linear equations:

$$\begin{bmatrix} \boldsymbol{R} & \mathbf{1} \\ \boldsymbol{F}^T & 0 \end{bmatrix} \begin{bmatrix} \boldsymbol{w} \\ -\mu / 2\sigma^2 \end{bmatrix} = \begin{bmatrix} \boldsymbol{r} \\ y_{lf}(\boldsymbol{x}) \end{bmatrix} \tag{9}$$

where

$$\boldsymbol{F}=\left[y_{lf}(\boldsymbol{x}^{(1)}),y_{lf}(\boldsymbol{x}^{(2)}),\cdots,y_{lf}(\boldsymbol{x}^{(n)})\right]^T \tag{10}$$

With the weight coefficient $\boldsymbol{w}$, we can get the HK predictor $\hat{y}(\boldsymbol{x})$ for any untried $\boldsymbol{x}$:

$$\hat{y}(\boldsymbol{x}) = \begin{bmatrix} \boldsymbol{r}(\boldsymbol{x}) \\ y_{lf}(\boldsymbol{x}) \end{bmatrix}^T \begin{bmatrix} \boldsymbol{R} & \boldsymbol{F} \\ \boldsymbol{F}^T & 0 \end{bmatrix}^{-1} \begin{bmatrix} \boldsymbol{y}_S \\ 0 \end{bmatrix} \tag{11}$$

The estimated value of HK model at any unknown position can be expressed as:

$$\hat{y}(\boldsymbol{x})=\beta_0\hat{y}_{lf}(\boldsymbol{x})+\boldsymbol{r}^T(\boldsymbol{x})\boldsymbol{R}^{-1}(\boldsymbol{y}_S-\beta_0\boldsymbol{F}) \tag{12}$$

where

$$\beta_0 = \left(\boldsymbol{F}^T\boldsymbol{R}^{-1}\boldsymbol{F}\right)^{-1}\boldsymbol{F}^T\boldsymbol{R}^{-1}\boldsymbol{y}_S \tag{13}$$

The MSE of the HK model is found to be:

$$MSE\left[\hat{y}(\boldsymbol{x})\right]=\sigma^2\left\{1.0-\boldsymbol{r}^T\boldsymbol{R}^{-1}\boldsymbol{r}+\left[\boldsymbol{r}^T\boldsymbol{R}^{-1}\boldsymbol{F}-y_{lf}(\boldsymbol{x})\right]\left(\boldsymbol{F}^T\boldsymbol{R}^{-1}\boldsymbol{F}\right)^{-1}\left[\boldsymbol{r}^T\boldsymbol{R}^{-1}\boldsymbol{F}-y_{lf}(\boldsymbol{x})\right]^T\right\} \tag{14}$$

From the above process of modeling, we can see that HK model introduces influence of low-fidelity function through the trend model. It can avoid difficult calculation of cross-covariance between the high-fidelity and low-fidelity level. Meanwhile, the dimensions of correlation matrix are reduced because of layering between different fidelity data. Fig 1 shows the optimization procedure based on HK model.

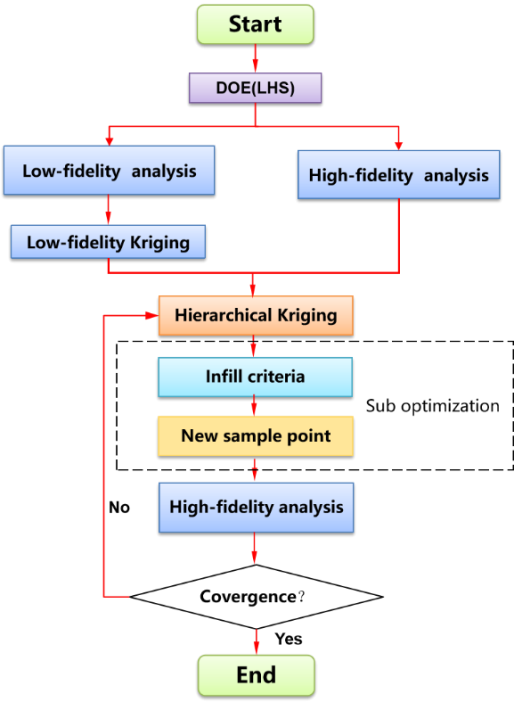

Fig 1 Optimization procedure with HK model

2.2 Multi-fidelity aerodynamic/stealth design optimization strategy

The framework of the multi-fidelity aerodynamic/stealth design optimization strategy developed in this paper is shown in Fig 2. There are two rounds in the process of optimization. In the first round, a low-fidelity aerodynamic/stealth design optimization with Kriging model is carried out. CFD/CEM simulations use low-fidelity methods such as RANS equations with coarse grids and PO method, which makes optimization computationally cheap. We can obtain a low-fidelity optimization shape in a short time and then analyses its aerodynamic and stealth performance with high-fidelity simulation. In the second round, a variable-fidelity design optimization with HK model is done. To make the full use of lots of data obtained in the previous step, we take all sample data obtained from the low-fidelity optimization as low-fidelity data of the variable-fidelity optimization. Meanwhile, Latin hypercube sampling (LHS) method, which is one of the most popular design of experiments (DoE) method, is used

to generate some new initial sample points. These new initial sample points are simulated with high-fidelity methods such as RANS equations with fine grids and MLFMA method. Both the new initial sample point data and the high-fidelity data that is obtained from optimum shape of low-fidelity optimization, are taken as high-fidelity data of the variable-fidelity optimization. HK model is applied to incorporate data with two levels of fidelity. Parallel infill-sampling method [19] is used to add new high-fidelity samples. Four kinds of infill criteria are performed at the same time，which are Minimizing Surrogate Prediction (MSP)，Expected Improvement (EI)，Prob-ability of Improvement (PI), and Lower-Confidence Bounding (LCB). All above has been included in an in-house optimization code named “SurroOpt” [10] [36]. Fig 3 shows the framework of“SurroOpt”. The work in this paper is studied with this optimization code.

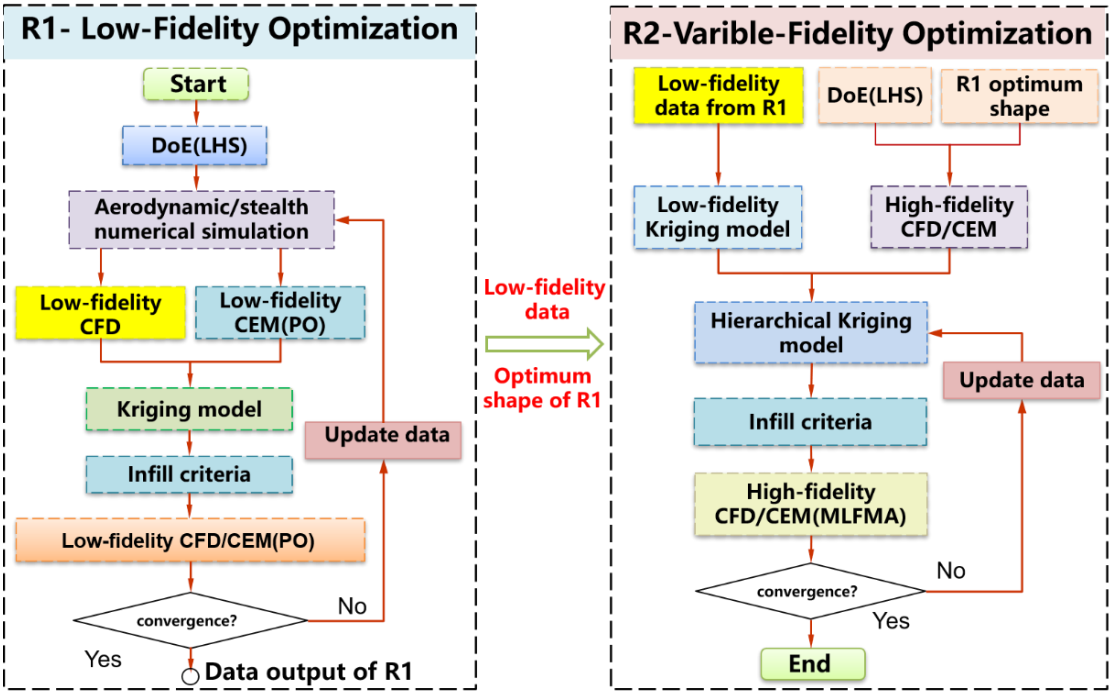

Fig 2 Framework of multi-fidelity aerodynamic/stealth design optimization strategy

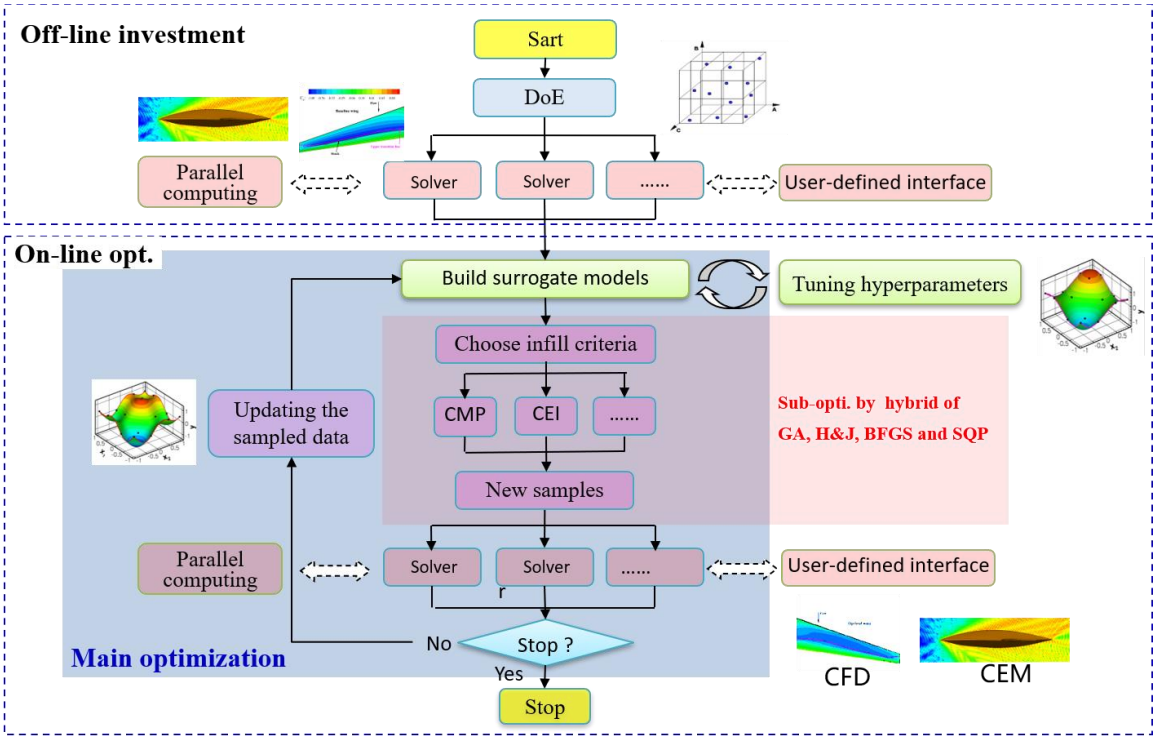

Fig 3 Framework of “SurroOpt”[36]

2.3 Validation of CFD solver

To validate the accuracy of CFD solver, we take the CRM configuration [37] as a validation example. The CFD solver used in this paper is named “PMNS3DR”, which is an in-house CFD code based on three-dimensional RANS equations and structured grid. RANS equations are spatially discretized by finite-volume method with JST scheme adopted, and LU-SGS method is used for time integration. Multigrid, local-time-stepping and variable-coefficient implicit residual smoothing are applied to accelerate convergence rate. In addition, S-A model is used for turbulence closure. The flow condition is $Ma=0.85, Re=5.0\times10^6, C_L=0.5$. The structured grid used for CFD simulation is shown in Fig 4. The comparison of computed pressure distribution and experimental data [37] is shown in Fig 5, where η represents the nondimensionalized spanwise coordinates. As can be seen, the calculated results agree well with the experimental results, except for the position $\eta=0.95$, which is due to the static aeroelastic effect of wing tip. The comparison proves that the CFD solver in the paper is reliable.

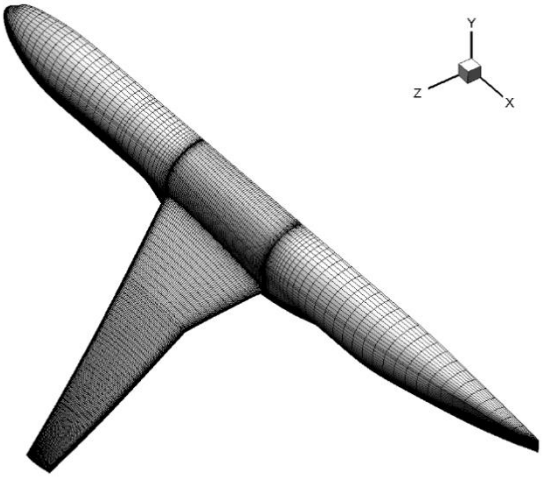

Fig 4 Sketch of surface grid for CRM configuration

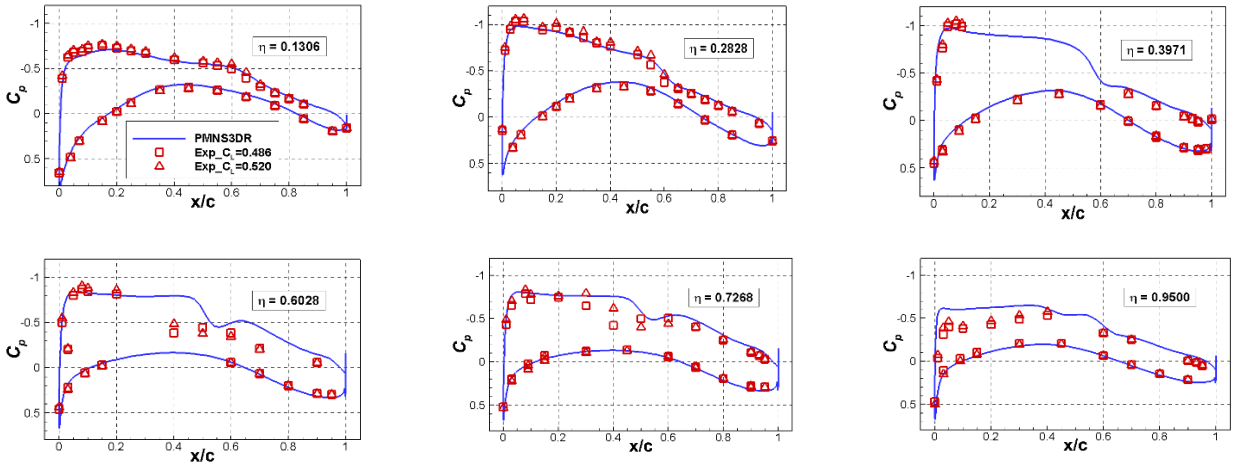

Fig 5 Comparison of computed pressure distribution and experimental data of CRM ($Ma=0.85, Re=5.0\times10^6, C_L=0.5$)

2.4 Validation of RCS prediction method

The goal of stealth optimization is to reduce the RCS of a target, which is defined as the following equation:

$$\sigma=4\pi \lim_{r\to\infty} r^2 \frac{|\boldsymbol{E}_s|^2}{|\boldsymbol{E}_i|^2} \tag{15}$$

where σ represents the RCS, $\boldsymbol{E}_s$ is the scatter electric field strength at the distance r from a target, a-nd $\boldsymbol{E}_i$ is the incident electric field strength at the target. The unit of RCS is square meters (m^2), but

we usually use decibels relative to a square meter (dBsm) to express it. The conversion relationship between them is as following:

$$\sigma_{dBsm} = 10\log\left(\sigma_{m^2}\right) \tag{16}$$

To calculate the σ in Eq. (15), we need to solve Maxwell equations as following:

$$\begin{aligned}
&\oiint_S \boldsymbol{D}\cdot d\boldsymbol{S} = \iiint_V \rho \mathrm{d}V \\
&\oiint_S \boldsymbol{B}\cdot d\boldsymbol{S} = 0 \\
&\oint_l \boldsymbol{E}\cdot d\boldsymbol{l} = -\frac{\partial}{\partial t}\iint_S \boldsymbol{B}\cdot d\boldsymbol{S} \\
&\oint_l \boldsymbol{H}\cdot d\boldsymbol{l} = \iint_S \boldsymbol{J} d\boldsymbol{S} + \frac{\partial}{\partial t}\iint_S \boldsymbol{D}\cdot d\boldsymbol{S}
\end{aligned} \tag{17}$$

where $\boldsymbol{E}$ is the electric field strength, $\boldsymbol{B}$ is the magnetic induction intensity, $\boldsymbol{H}$ is the magnetic field strength, $\boldsymbol{D}$ is the electric displacement vector, $\boldsymbol{J}$ is the current density, and ρ is the electric charge density. Based on Eq. (17), we can get the electronic field integral equation (EFIE) described in Eq. (18) and the magnetic field integral equation (MFIE) described in Eq. (19):

$$-\frac{j}{\omega\mu}\hat{\boldsymbol{n}}\times\boldsymbol{E}_i(\boldsymbol{r}) = \hat{\boldsymbol{n}}\times\int_S\left[\boldsymbol{J}(\boldsymbol{r}')G(\boldsymbol{r},\boldsymbol{r}') + \frac{1}{k^2}\left(\nabla\cdot\boldsymbol{J}(\boldsymbol{r}')\right)\left(\nabla G(\boldsymbol{r},\boldsymbol{r}')\right)\right]d\boldsymbol{S}' \tag{18}$$

$$\hat{\boldsymbol{n}}\times\boldsymbol{H}_i(\boldsymbol{r}) = -\left(1-\frac{\Omega}{4\pi}\right)\boldsymbol{J}(\boldsymbol{r}) + \hat{\boldsymbol{n}}\times\int_s \boldsymbol{J}(\boldsymbol{r}')\times\nabla G(\boldsymbol{r},\boldsymbol{r}')d\boldsymbol{S}' \tag{19}$$

where Ω is the solid angle of tangent at observation point on surface. Then, we can get the surface current $\boldsymbol{J}$ to calculate the scatter electric field strength $\boldsymbol{E}_s$ and the incident electric field strength $\boldsymbol{E}_i$. With the aim of making convergence of RCS calculation better for three-dimensional complex shape, the combined field integral equation (CFIE) [5] is used in the paper. It is described as following:

$$\mathrm{CFIE} = \alpha\mathrm{EFIE} + (1-\alpha)\mathrm{MFIE} \quad (0<\alpha<1) \tag{20}$$

α is the combined field factor which is 0.2 in the paper. Among the RCS prediction methods, MLFMA and PO are the most common methods to solve Eq. (20). MLFMA [38] is a kind of frequency-domain method which is accurate but need lots of memory and time costs. PO [6] is a high-frequency approximation algorithm which is fast and requires less memory, but it is not accurate especially for the shape with large curvature edge. As for the material of stealth target, perfect electric conductor (PEC) is assumed in the current study.

The double-ogive model, which is a benchmark model for CEM, is adopted to validate the CEM solver used in the paper. For one half-ogive, the half angle at tip is 46.4 deg and the length is 2.5 in. For another half-ogive, the half angle at tip is 22.62 deg and the length is 5 in. The frequency of incident wave is 9GHz and both horizontal and vertical polarizations are calculated. The average length of the triangle facets is $\lambda/16$. Fig 6 shows the directions of incident radar wave and the shape of double-ogive model. The calculation methods are MLFMA and PO.

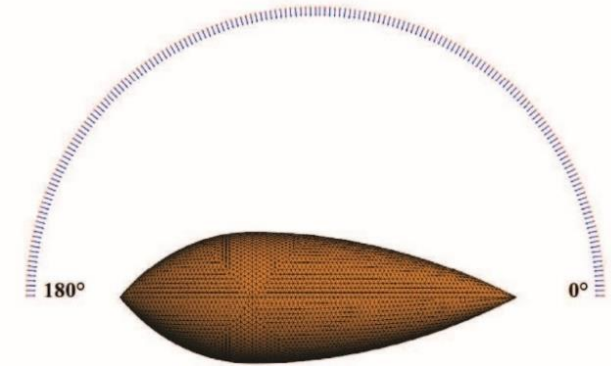

Fig 6 Directions of incident radar wave

The comparison of computational results and experimental data is shown in Fig 7. We can see that the result of MLFMA is in good agreement with the experimental data for both horizontal and vertical polarizations. At the tips of double-ogive, the accuracy of PO method is poor compared with the experimental data because of its physics assumption. In the middle of double-ogive where curvature of the surface is small, PO method can capture the trend of RCS well. The results prove that the CEM solver used in present paper is reliable.

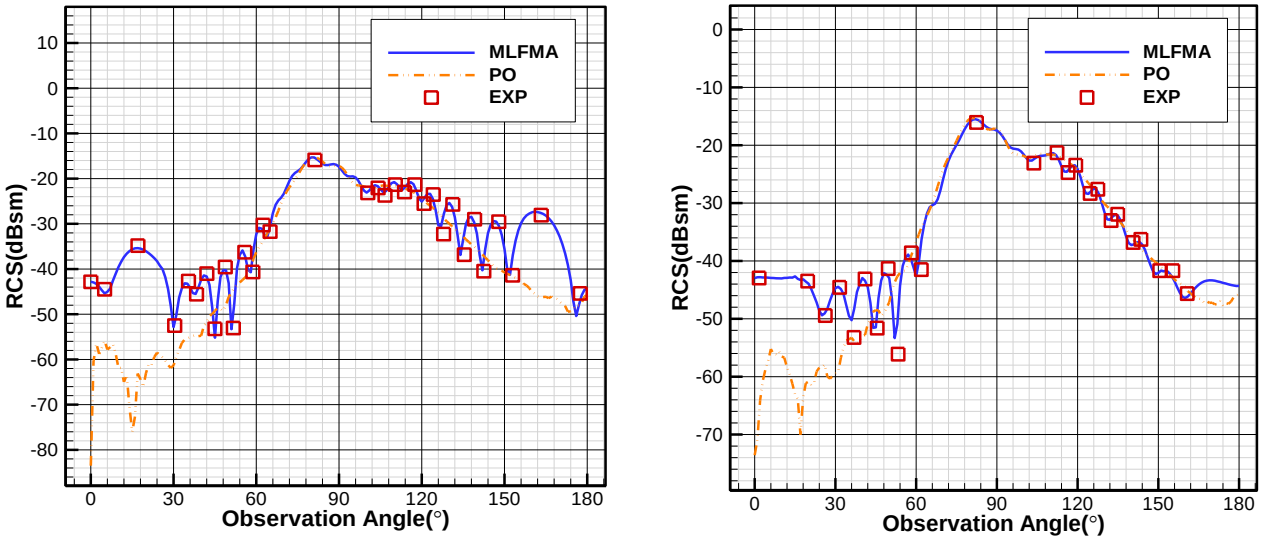

(a) HH polarization (b) VV polarization

Fig 7 Radar cross section for double-give at frequency 9GHz

3. Aerodynamic/Stealth Shape Design Optimization of Flying Wing

3.1 Problem statement of design optimization

The detailed geometry parameters of baseline shape is shown in Fig 8. The initial geometry has a span of 18.92m and the length of fuselage is 11.63m. Geometric parameters of configuration are shown in the Table 1. Free form deformation (FFD) method [39] is used to parameterize the shape of flying wing. The corresponding FFD control volume is shown in Fig 9. The control points are divided into two layers. At each layer, there are 10 points streamwise and 6 points spanwise. We make the X coordinates and the Z coordinates of each control points unchanged. At the same time, Y coordinates of 6 points at the trailing edge of each layer are also remained unchanged. Only other 54 points of Y coordinates along streamwise are taken as design variables at each layer. There are 108 design variables in total.

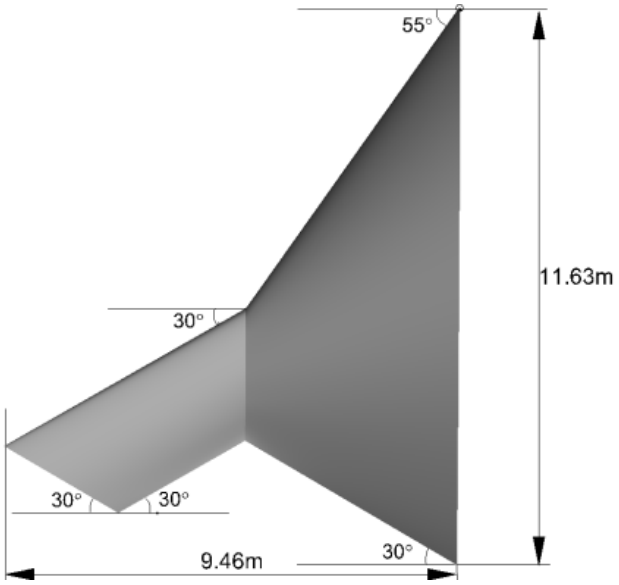

Fig 8 Baseline shape of a flying wing aircraft

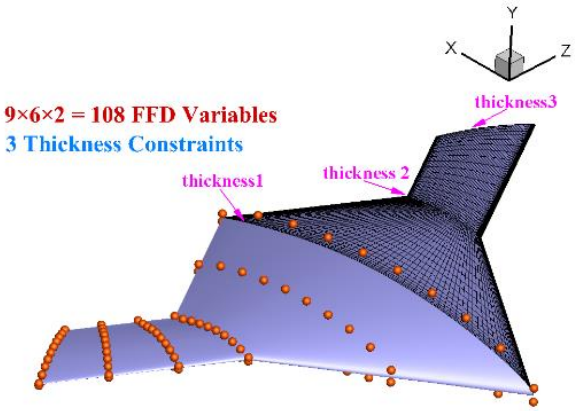

Fig 9 FFD control volume of a flying wing aircraft

Table 1 Geometric parameters of a flying wing configuration

Geometric parameter	Value
Span (m)	18.92
Length (m)	11.63
Sweep angle（°）	55/30
Reference wing area (m^2)	84.42
Reference center (m)	(6.143, 0. 0)
Mean aerodynamic chord (m)	6.687

The aim of shape design optimization is to reduce drag of cruise condition and frontal RCS. The aerodynamic and electromagnetic computational states are shown in the Table 2. The coordinate system for the directions of incident radar wave is shown in Fig 11.The observation angle range used in the paper is $\varphi=90^\circ$, $\phi=0\sim180^\circ$. The optimization problem formulation is described as following, which with constrains of lift coefficient, pitching moment, and maximum thicknesses at three spanwise sections:

$$\begin{aligned} min. \quad & w_1\left(\frac{C_D}{C_{D0}}\right)+w_2\left(\frac{\overline{RCS}_{0\sim60^\circ VV}}{\overline{RCS_0}}\right) \\ & w_1=0.8,\ w_2=0.2 \\ s.t. \quad & C_{\mathrm{L}}=0.2 \\ & \left|C_M\right|\le 0.001 \\ & t_n \ge t_{n\text{-}low}\ \left(n=1,2,3\right) \end{aligned} \tag{21}$$

where C_D is the drag coefficient of flying wing at the cruise condition. C_{D0} is the drag coefficient of baseline shape. $\overline{RCS}_{0\sim60^\circ VV}$ is average RCS in the observation angle range $\phi=0\sim60^\circ$. $\overline{RCS_0}$ is the corresponding RCS value of the baseline shape. C_{L} is the cruise lift coefficient. C_M is pitching moment coefficient about the reference center. w_1 and w_2 are weight coefficients of the aerodynamic and stealth objectives. $t_n\left(n=1,2,3\right)$ is the maximum thickness of different key position along the wing span. There are three key positions where the maximum thickness need to be constrained. They are shown in Fig 10, $t_{n\text{-}low}\left(n=1,2,3\right)$ is the maximum thicknesses of baseline shape in the sec1,sec2 and sec3.

Table 2 Computational states of aerodynamic/stealth design optimization

Parameter	Value
Cruise Mach number	0.75
Cruise lift coefficient	0.2
Reynolds number	4.26 x 10^7
Incident wave frequency(GHz)	1
Polarization mode	VV

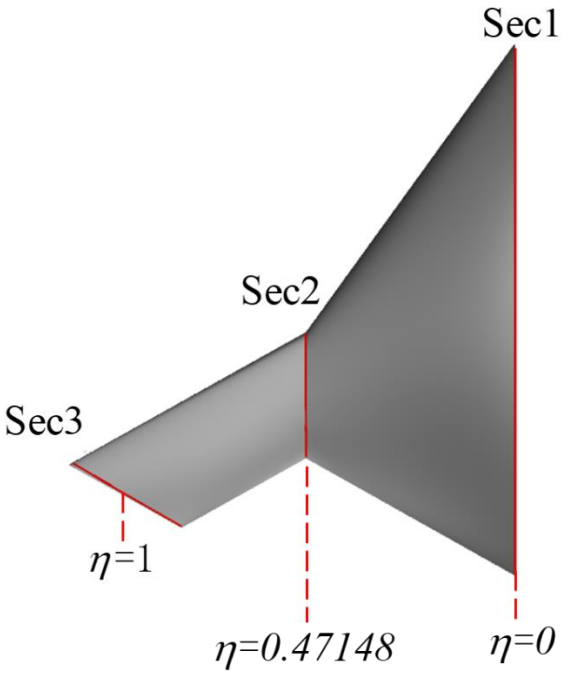

Fig 10 Sections where the maximum thickness need to be constrained

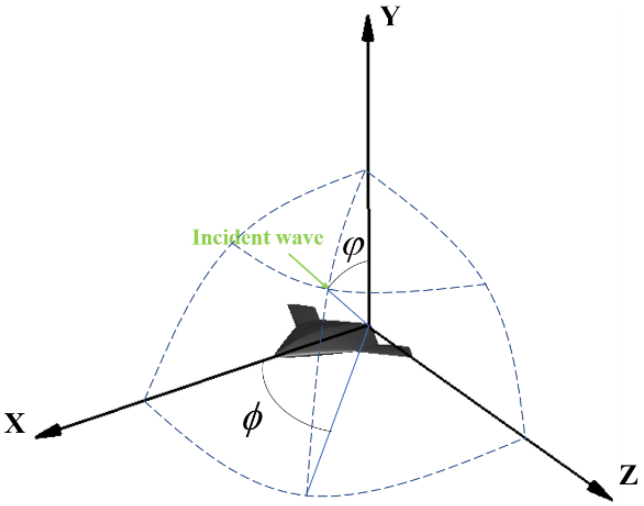

Fig 11 Definition of the coordinate system

3.2 Selection of high-fidelity and low-fidelity analysis model

Selection of high-fidelity and low-fidelity simulation methods is crucial for variable-fidelity optimization. In this paper, RNAS equations with coarse grid are used as low-fidelity CFD simulation and PO algorithm is used as low-fidelity CEM simulation. As for the methods of high-fidelity CFD and CEM, RNAS equations with fine grid are used as high-fidelity CFD simulation and MLFMA algorithm is used as high-fidelity CEM simulation. The CFIE equation with the combined field factor $\alpha=0.2$ is solved to calculate RCS.

A grid convergence study is carried out to determine the grids for high-fidelity and low-fidelity CFD simulations. There are five levels used for grid convergence study. Fig 12 shows the partial grid levels. Fig 13 and Table 3 show the drag coefficient and computational time varied with the number of grids. As shown in Table 3, the change of drag coefficient is smaller than 1 counts when the grid size is larger than 4560000. Thus, L1 grid is used for high-fidelity CFD simulation and L3 is used for low-fidelity CFD simulation.

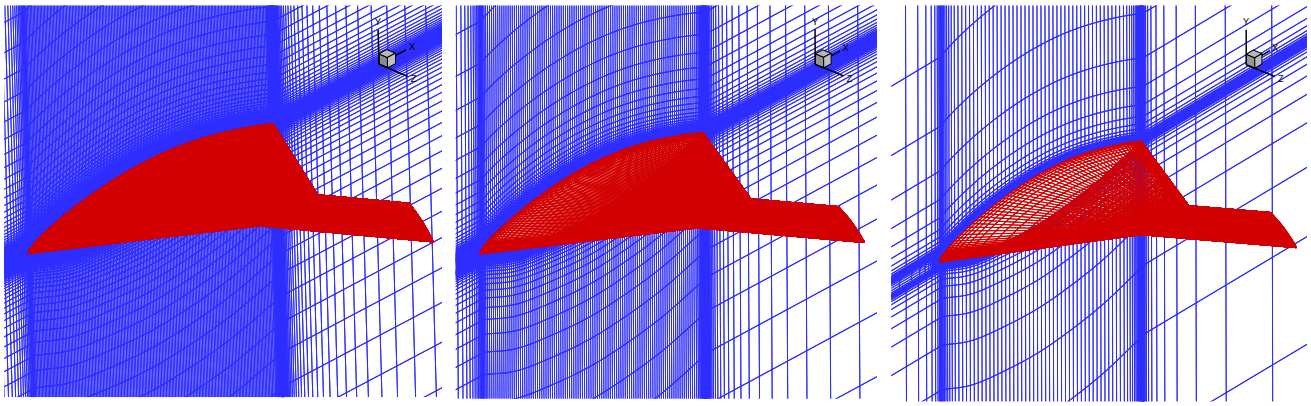

(a) L0 grid (b) L1 grid (C) L3 grid

Fig 12 Comparison of different grids

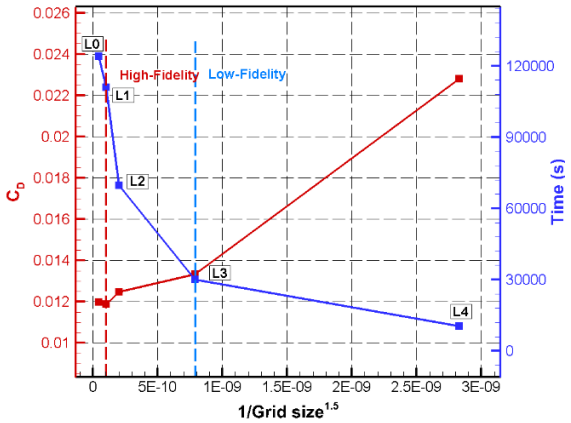

Fig 13 Drag coefficient and time varied with the number of grids

Table 3 Grid convergence study for the baseline shape

Grid level	Grid size	CL	CD(cts)	Relative CPU time
L0	8000000	0.2	119.88	1
L1	4560000	0.2	118.90	0.895
L2	2900000	0.2	124.77	0.563
L3	1170000	0.2	133.41	0.242
L4	500000	0.2	227.98	0.083

In the process of low-fidelity optimization in the first round, LHS method is used to generate 110 initial sample points. Minimizing Surrogate Prediction (MSP)，Expected Improvement (EI)，Probability of Improvement (PI), and Lower-Confidence Bounding (LCB) are implemented. When the number of sample points is up to 492, the low-fidelity optimization is finished. At the begin of variable-fidelity optimization in the second round, LHS method is used to generate 10 new initial sample points which are simulated with high-fidelity CFD/CEM methods. The optimum shape of low-fidelity optimization is also simulated with high-fidelity CFD/CEM methods to generate the corresponding high-fidelity data. Thus, there are 11 high-fidelity initial sample points and 492 low-fidelity initial sample points in the variable-fidelity optimization.

3.3 Design results and discussion

After the low-fidelity optimization, the aerodynamic and stealth performance of the optimum shape is calculated by high-fidelity CFD/CEM method, which is shown in Table 4 and served as high-fidelity data to build HK model. Fig 14 and Fig 15 show the convergence process of the multi-fidelity aerodynamic/stealth design optimization. As the comparison, a high-fidelity optimization with Kriging model is carried out. The number of initial sample points is 10. Fig 14 shows the objective value varied with the number of low-fidelity CFD/CEM in the low-fidelity optimization. Fig 15 shows the objective value varied with the number of high-fidelity CFD/CEM. The method developed in the paper and traditional high-fidelity optimization with Kriging model is compared in Fig 15. The legend “HK” represents the method developed in the paper and the legend “Kriging” represents high-fidelity optimization with Kriging model. We can see that the method developed in the paper can significantly accelerate the convergence of optimization. Table 5 shows evaluation number of high-fidelity CFD/CEM required by the different optimization methods. As we can see, method developed in this paper only need 39 high-fidelity CFD/CEM simulations to get the optimum shape. However, the traditional high-fidelity optimization with Kriging model requires 285 high-fidelity CFD/CEM simulations and the results are not as good as the HK method. The number of high-fidelity CFD/CEM simulations which is time-consuming, is reduced by a factor of 7.

Table 4 High-fidelity CFD/CEM simulation results of the first-round optimum shape

	C_L	C_D(cts)	C_M	$RCS_{average}$ (m^2)	t_1(m)	t_2(m)	t_3(m)
Baseline	0.2	118.924	-0.0006	1.1389	1.985	0.369	0.138
Optimum	0.2	115.057	0.00007	0.7634	1.985	0.371	0.139

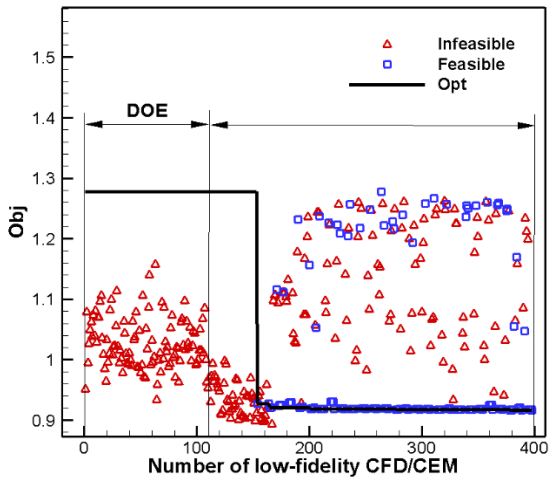

Fig 14 convergence process of low-fidelity optimization

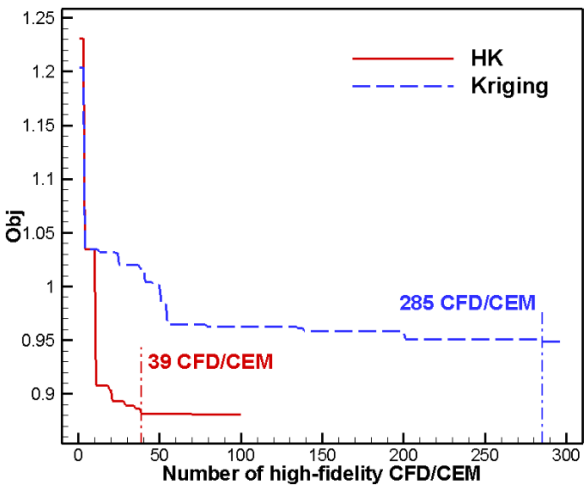

Fig 15 convergence process of variable-fidelity optimization

Table 5 Calculation costs of different optimization methods

Method	Objective value	Number of high-fidelity CFD/CEM
HK	0.8814	39
Kriging	0.9485	285

Fig 16 shows the pressure distributions on the upper surface of the baseline (lift) and the optimum (right). Fig 17 shows geometry and pressure distributions at different sections of the baseline and the optimum. η represents the nondimensionalized spanwise coordinates. The strength of shock wave at the outer wing is reduced after optimization and the radius of the leading edge is reduced. Fig 18 shows the RCS comparisons of the baseline and the optimum. The RCS of the optimum in the range $\phi=0\sim180^{\circ}$, $\varphi=90^{\circ}$ is reduced compared with the baseline. In the range $\phi=90\sim120^{\circ}$ and $\phi=150\sim180^{\circ}$, RCS value is significantly reduced. Table 6 shows the design objective and constraints of the optimum shape. As we can see, drag coefficient of flying wing at the cruise condition is reduced by 3.5% and average RCS in the observation angle range is reduced by 44.3%. All constraints, including lift coefficient, pitching moment coefficient, and maximum thicknesses at three spanwise sections, are satisfied.

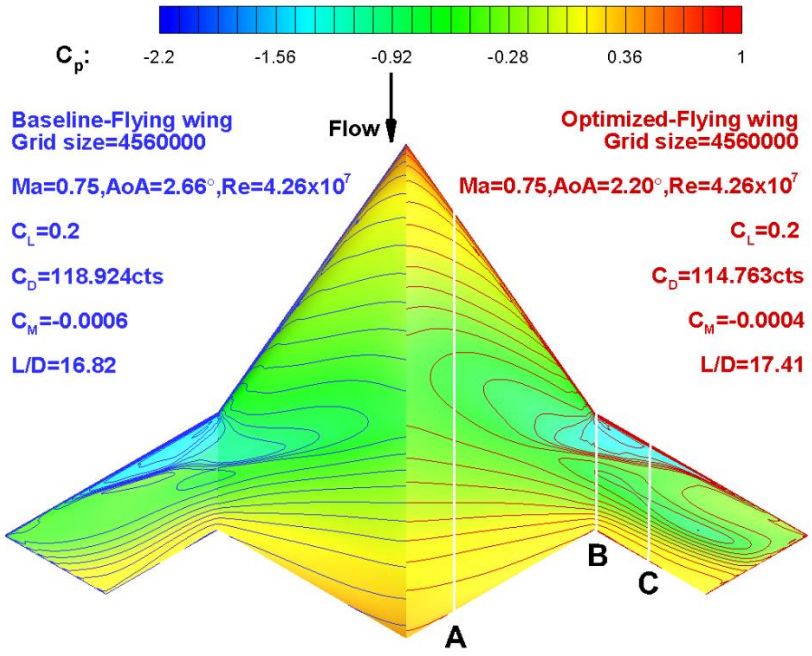

Fig 16 pressure distributions on upper surface of the baseline shape and the optimum shape

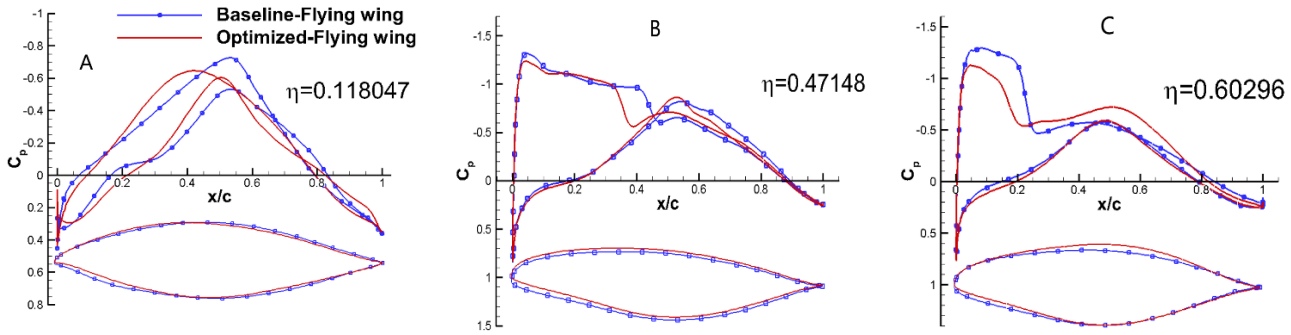

Fig 17 Geometry and pressure distributions at different section of baseline and optimum shape ($Ma=0.75, Re=4.26\times10^7, C_L=0.2$)

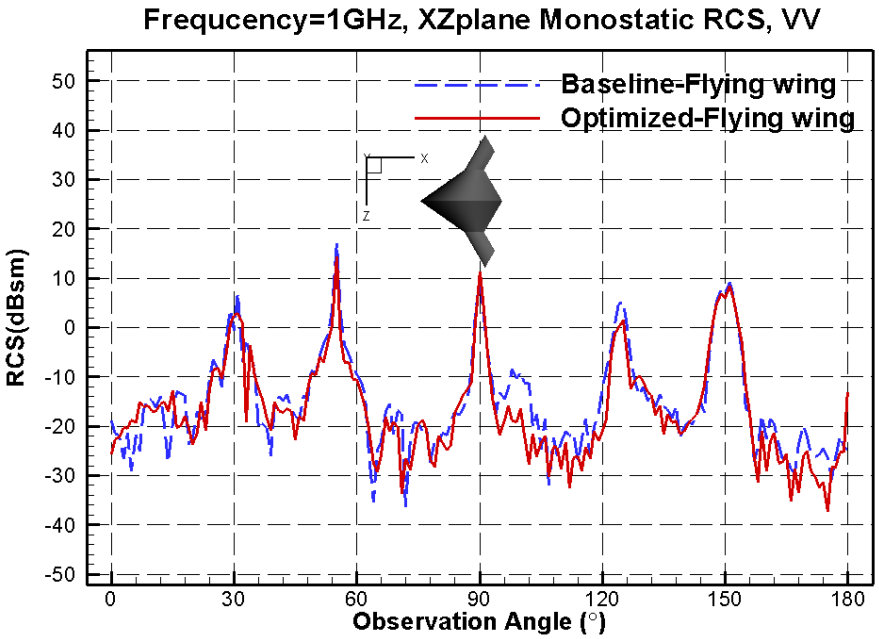

Fig 18 RCS comparisons of the baseline and optimum shape (0~180° VV)

Table 6 Comparisons of design objective and constraints between the optimum and the baseline

	C_L	C_D(cts)	C_M	$RCS_{average}$ (m^2)	t_1(m)	t_2(m)	t_3(m)
Baseline	0.2	118.924	-0.0006	1.1389	1.985	0.369	0.138
Optimum	0.2	114.763	-0.0004	0.6344	2.005	0.370	0.140
Δ	/	-3.5%	/	-44.3%	/	/	/

4. Conclusions

In order to improve efficiency of the global aerodynamic/stealth design optimization for three-dimensional complex shape with more than 100 design variables, a two-rounds multi-fidelity aerodynamic/stealth design optimization method based on HK model is developed in this paper. MLFMA and PO, which are two kinds of CEM simulation methods with different accuracy, are combined with HK model. Improved flying wing shapes are obtained via numerical optimization, effectively reducing the drag coefficient and RCS. Through the analysis of the optimization process and results, the following conclusions are reached:

(1) The two-rounds multi-fidelity aerodynamic/stealth design optimization method based on HK model can greatly improve the optimization efficiency of high dimensional aerodynamic/ stealth optimization problem. In the present case, with the assistance of low-fidelity sample points, only 39 high-fidelity CFD/CEM simulations are used to get the optimum shape for the

flying wing aerodynamic/stealth optimization with 108 design variables. As a comparison, traditional optimization method with Kriging model and high-fidelity CFD/CEM simulation needs 285 high-fidelity CFD/CEM simulations. The number of high-fidelity CFD/CEM simulations decrease by seven times.

(2) 108 design variables are used for the global aerodynamic/stealth design optimization of a flying wing aircraft. The drag coefficient of optimized flying wing at a cruise condition is reduced by 3.5%. The average RCS in the frontal observation angle range is reduced by 44.3%, much lower than that of the baseline flying wing under all constraints. The stealth performances in other observation angle range such as side direction and backward direction are also improved.

The future work beyond the scope of this article will focus on aerodynamic/stealth design optimization considering the wide-Mach-number-range aerodynamic performance and wide-radar wave-band stealth performance.

5. Acknowledgments

This research was supported by the National Natural Science Foundation of China grant (Nos. 11972305, 12072285 and 11772261) and Shaanxi Science Fund for Distinguished Youth Scholars under grant number of 2020JC-13.

6. Contact Author Email Address

Zi-Qiao Liu, M.Phil Student, ziqiaoliu@mail.nwpu.edu.cn.

Wen-Ping Song, Professor, wpsong@nwpu.edu.cn

Zhong-Hua Han*, Professor, hanzh@nwpu.edu.cn, corresponding author.

7. Copyright Statement

References

[1] Jameson A. Aerodynamic design via control theory [J]. Journal of scientific computing, 1988, 3(3):23360.

[2] Bai J Q, Lei R W, Yang T H, et al. Progress of Adjoint-Based Aerodynamic Optimization Design for Large Civil Aircraft[J]. Acta Aeronautica et Astronautica Sinica, 2019, 40(1):522642 (in Chinese).

[3] Huang T J, Liu G, Gao Z H, et al. Current Situation and Development Trend of Multidisciplinary Coupled Adjoint System in Aircraft Multidisciplinary Optimization[J]. Acta Aeronautica et Astronautica Sinica, 2020, 41(3):623404 (in Chinese).

[4] Wang L, and Anderson W K. Adjoint-Based Shape Optimization for Electromagnetic Problems Using Discontinuous Galerkin Methods[J]. AIAA Journal, 2011, 49(6):1302-1305.

[5] Zhou L, Huang J T, Gao Z H, et al Three-Dimensional Aerodynamic/Stealth Optimization Based on Adjoint Sensitivity Analysis for Scattering Problem[J]. AIAA Journal, 2020, 58(6):2702-2715.

[6] Li M, Bai J Q, Li L, et al A Gradient-Based Aero-Stealth Optimization Design Method for Flying Wing Aircraft[J]. Aerospace Science and Technology, 2019, 92:156-169.

[7] Mäkinen R A E, Periaux J, and Toivanen J. Multidisciplinary Shape Optimization in Aerodynamics and Electromagnetics Using Genetic Algorithms[J]. International Journal for Numerical Methods in Fluids, 1999, 30(2):149-159.

[8] Lee D S, Gonzalez L F, Srinivas K. Robust Evolutionary Algorithms for UAV/UCAV Aerodynamic and RCS Design Optimization[J]. Computers and Fluids, 2008, 37(5):547-564.

[9] Xia L, Zhang X, Yang M H, et al. Airfoil Aerodynamic Stealth Integrated Design for a Flying Wing Configuration[J]. Journal of Northwestern Polytechnical University, 2017, 35(5):821-826.

[10] Han Z H, Xu C Z., Qiao J L, et al. Recent Progress of Efficient Global Aerodynamic Shape Optimization Using Surrogate-Based Approach[J]. Acta Aeronautica et Astronautica Sinica, 2020, 41(3): 623344(in Chinese).

[11] Han Z H. Kriging Surrogate Model and Its Application to Design Optimization: A Review of Recent Progress[J]. Acta Aeronautica et Astronautica Sinica, 2016, 37(11):3197-3225 (in Chinese).

[12] Liu F, Han Z H, Zhang,Y, et al. Surrogate-Based Aerodynamic Shape Optimization of Hypersonic Flows Considering Transonic Performance[J]. Aerospace Science and Technology, 2019, 93(10):105345.

[13] Wu M M, Han Z H, Nie H, et al. A Transition Prediction Method for Flow over Airfoils Based on High-order Dynamic Mode Decomposition[J]. Chinese Journal of Aeronautics, 2019, 32(11):2408-2421.

[14] Zhang K S, Han Z H, Gao Z J, et al. Constraint Aggregation for Large Number of Constraints in Wing Surrogate-Based Optimization[J]. Structural and Multidisciplinary Optimization, 2019, 59(2):421-438.

[15] Han Z H, Chen J, Zhang K S, et al. Aerodynamic Shape Optimization of Natural-Laminar-Flow Wing Using Surrogate-Based Approach[J]. AIAA Journal, 2018, 56(7):2579-2593.

[16] Han Z H, Abu-Zurayk M., Goertz S, et al. Surrogate-Based Aerodynamic Shape Optimization of a Wing-Body Transport Aircraft Configuration. In Heinrich R. (eds) AeroStruct: Enable and Learn How to Integrate Flexibility in Design[C]. AeroStruct 2015. Notes on Numerical Fluid Mechanics and Multidisciplinary Design. 2018, 138:257-282.

[17] Xu C Z., Han Z H, Zhang K S, et al. Surrogate-Based Optimization Method Applied to Multidisciplinary Design Architectures[C]. ICAS 2018-0496, 31st Congress of the International Council of the Aeronautic Sciences, Sep. 9-14, 2018, Belo Horizonte, Brazil.

[18] Han Z H, Zhang Y, Song C X, et al. Weighted Gradient-Enhanced Kriging for High-dimensional Surrogate Modeling and Design Optimization[C]. AIAA Journal, 2017, 55(12):4330-4346.

[19] Liu J, Song W P, Han Z H, et al. Efficient Aerodynamic Shape Optimization of Transonic Wings Using a Parallel Infilling Strategy and Surrogate Models[J]. Structural and Multidisciplinary Optimization, 2017, 55(3):925-943.

[20] Han Z H, Zhang Y, Xu C.Z, et al. Aerodynamic Shape Optimization of Large Civil Aircraft Wing using Surrogate Model[J]. Acta Aeronautica et Astronautica Sinica, 2019, 40(1):522398-522398 (in Chinese).

[21] Han S Q, Song W P, Han Z H, et al. Aerodynamic Inverse Design Method based on Gradient-Enhanced Kriging Model[J]. Acta Aeronautica et Astronautica Sinica, 2017, 38(7):138-152 (in Chinese).

[22] Han S Q, Song W P, Han Z H, et al. Hybrid Inverse/Optimization Design Method for Rigid Coaxial Rotor Airfoils Considering Reverse Flow[J]. Aerospace Science and Technology, 2019, 95(12):105488.

[23] Bu Y P, Song W P, Han Z H, et al. Aerodynamic/Aeroacoustic Variable-Fidelity Optimization of Helicopter Rotor Based on Hierarchical Kriging Model[J]. Chinese Journal of Aeronautics, 2020, 33(2):476-492.

[24] Qiao J L, Han Z H, and Song W P. An Efficient Surrogate-Based Global Optimization for Low Sonic Boom Design[J]. Acta Aeronautica et Astronautica Sinica, 2018, 39(5):67-80 (in Chinese).

[25] Zhang W, Gao Z H, Zhou L, et al. Efficient Surrogate-Based Aerodynamic Shape Optimization with Adaptive Design Space Expansion[J]. Acta Aeronautica et Astronautica Sinica, 2020, 41(10):123815 (in Chinese).

[26] Zhang B Q, Luo L, Chen Z L, et al. Stealth Airfoil Optimization for Flying Wing Configuration[J]. Acta Aeronautica et Astronautica Sinica, 2014, 35(4):957-967.

[27] Jiang X W, Zhao Q J, Zhao G Q, et al. Integrated Optimization Analyses of Aerodynamic/Stealth Characteristics of Helicopter Rotor Based on Surrogate Model[J]. Chinese Journal of Aeronautics, 2015, 28(3):737-748.

[28] Han Z H, Goertz S, and Zimmermann R. Improving Variable-Fidelity Surrogate Modeling via Gradient-Enhanced Kriging and a Generalized Hybrid Bridge Function[J]. Aerospace Science and Technology, 2013, 25(1):177-189.

[29] Zhang D H, Gao Z H, Li J Z, et al. Aerodynamic and Stealth Synthesis Design Optimization of UAV Based on Double-Stage Metamodel[J]. Acta Aerodynamica Sinica, 2013, 31(3):394-400.

[30] Gao Z H, Wang M L. An Efficient Algorithm for Calculating Aircraft RCS Based on the Geometrical Characteristics[J]. Chinese Journal of Aeronautics, 2008, 21(4):293-303.

[31] Han Z H, Zimmermann R, and Goertz S. Alternative Cokriging Model for Variable-Fidelity Surrogate Modeling[J]. AIAA Journal, 2012, 50(5):1205-1210.

[32] Han Z H, Goertz S. Hierarchical Kriging Model for Variable-Fidelity Surrogate Modeling[J]. AIAA Journal, 2012, 50(9):1885-1896.

[33] Kennedy M C, O'Hagan A. Predicting the Output from a Complex Computer Code When Fast Approximations Are Available[J]. Biometrika, 2000, 87(1):1-13.

[34] Han Z H, Xu C Z, Zhang L, et al. Efficient Aerodynamic Shape Optimization Using Variable-Fidelity Surrogate Models and Multilevel Computational Grids[J]. Chinese Journal of Aeronautics, 2020, 33(1):31-47.

[35] Zhang L, Zhou Z, Xu X P. Integrated Design on Aerodynamic and Stealthy of Flying Wing Unmanned Ae-

rial Vehicle Based on Stealthy Inverse Design Method[J]. Journal of Harbin Institute of Technology, 2017, 49(10):22-30.

[36] Han Z H. SurroOpt: A Generic Surrogate-based Optimization Code for Aerodynamic and Multidisciplinary Design[C]. ICAS 2016-0281, 30th Congress of the International Council of the Aeronautical Sciences, Sep.25-30, 2016, Daejeon, South Korea.

[37] Levy D W, Laflin K R, Tinoco E N, et al. Summary of Data from the Fifth Computational Fluid Dynamics Drag Prediction Workshop[J]. Journal of Aircraft, 2014, 51(4): 1194-1213.

[38] Pan X M, Sheng X Q. A Sophisticated Parallel MLFMA for Scattering by Extremely Large Targets[J]. IEEE Antennas and Propagation Magazine, 2008, 50(3):129-138.

[39] Sederberg T W, Parry S R. Free-Form Deform of Solid Geometric Models[J]. Computer Graphics, 1986, 20(4): 151-160.